Journal of Colloid and Interface Science 448 (2015) 287–296

Contents lists available at ScienceDirect

Journal of Colloid and Interface Science

www.elsevier.com/locate/jcis

Buckling of particle-laden interfaces

Theo D. Kassuga, Jonathan P. Rothstein *

University of Massachusetts Amherst, Mechanical and Industrial Engineering Department, United States

GRAPHICAL ABSTRACT

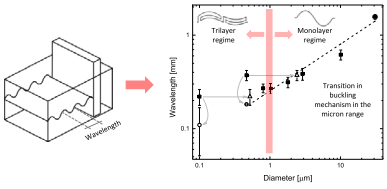

ARTICLE INFO

Article history:
Received 3 November 2014
Accepted 3 February 2015
Available online 11 February 2015

Keywords:
Particle-laden interfaces
Wavelength of buckling
Cascading
Hysteresis

ABSTRACT

In this paper, we investigate the buckling of an oil–water interface populated by micron-sized latex particles using a Langmuir trough. In this work, we extend results of buckling of particle-laden interfaces from the millimeter down to the submicron range while investigating the effect of a different capillary length on the resulting wavelength. The experimental data is compared to the existing theoretical framework. An unexpected deviation from the prediction of theory of the dominant wavelength of buckling is observed for particles smaller than one micron. Those observations suggest that there is a transition to a new buckling regime involving the formation of trilayers below one micron. For the first time in particle rafts, cascading of the dominant wavelength similar to that observed in thin polymer films is reported. In addition a series of transitions between wavelengths not observed in thin films is observed within the same particle raft. Lastly, the effect of compression history on the macroscopic arrangement of particles is investigated, along with its effect on the buckling wavelength.

1. Introduction

Particle-laden interfaces have found wide application in modern industry [1]. In particular, particles on interfaces have been widely used in industry, consumer products and foods to stabilize emulsions. This concept was originally proposed in the beginning of the 20th century [2] and is often given the name "Pickering emulsions".

A few factors lead to the ability of particles to stabilize emulsions. First, coalescence between drops is hindered by the presence of solids on the interfaces. Furthermore, Ostwald ripening can stop as the surface coverage ratio of smaller drops becomes higher and the effective surface tension decreases. Thus, a particle-stabilized emulsion tends to an equilibrium state where all the drops are at approximately the same Laplace pressure [3]. It has also been suggested that the elasticity of the particle shell around each drop could also help halt ripening by resisting compression of the drop interface [1]. As a result, particles and surfactant molecules have very similar effects on the behavior of the interface [1].

Besides stabilizing emulsions, it has been shown that particles can be used to create self-assembled capsules, for example by using a liquid jet as a template [4,5]. This opens the possibility of using particle-laden interfaces for encapsulation of active ingredients, such as drugs, by creating small, self-assembled capsules [6].

However, self-assembly is not limited to curved capsules and indeed flat surfaces of different properties can be manufactured this way. It is particularly interesting that using particles of different surface treatments and of different sizes, one can control the way they pack on the interface and thus modify the properties of the resulting solid material [7]. Naturally, that raises the question of how particles interact on the interface. This question is

* Corresponding author.
E-mail address: rothstein@ecs.umass.edu (J.P. Rothstein).

http://dx.doi.org/10.1016/j.jcis.2015.02.012
0021-9797/

fundamental not just for self-assembly, but also to understand the drop in surface pressure due to the presence of particles. In fact, particle–particle interactions is a rich field that gives insight on very interesting physics. On a very simplified level, particles interact through long and short range forces, which can be either repulsive or attractive. Because a number of forces are at play at any given time (gravity, surface tension, Coulombic attraction and repulsion, electrodipping, van der Waals, etc.) and they depend on a number of factors including the distance between the particles [8], it is natural to expect that the nature of these interactions can change as the packing of particles is modified.

Capillary interactions between multiple objects floating on an interface can lead to their self-assembly and the formation of particle rafts [9–13]. For a dense object with a large contact angle floating on the surface of a liquid, the weight of the particle can deform the fluid interface downward in such a way that the gravitation potential energy has been shown to decrease as the objects approach [14]. The result is an attractive force which scales like the inverse of particle separation and causes the floating objects to self-assemble [14]. For colloidal particles, the weight of the particle becomes too small to significantly deform the fluid interface and the gravitational forces become inconsequential. Even in the absence of gravity, however, attractive interactions between particles have been observed [15]. These attractive interactions can originate from interface deformation resulting from the electrostatic forces from a charged particle which can introduce a normal force acting on the oil water interface [9] or alternatively from immersion capillary forces resulting from non-uniform wetting [14–16]. Both these phenomena can result in particle aggregation into dense clusters [16]. In addition, for these small particles suspended on a water–oil or water–air interface, Coulomb interactions tangent to the interface can result in a repulsive force between particles that can often lead to their assembly into well-ordered hexagonal crystalline lattices [17–19].

The end result of such complex interactions is that particle-laden interfaces can have very interesting elastic behavior, particularly in shear and compression. In fact, the elasticity of the interface has been measured in a number of ways, such as by compression of flat interfaces [10] or by measuring surface pressure isotherms in particle-laden droplets [20]. Furthermore, as the interface is compressed the packing density increases and eventually reaches a maximum where particles can no longer rearrange on the interface. At this point, the surface tension goes to zero, as the repulsive and attractive interactions cancel each other [20,21]. Because the particles cannot rearrange, further compression of the interface must either lead to compressive deformation of the particles themselves or out-of-plane deformation, or buckling, of the interface. Whether an interface buckles depends on whether, at a given strain, it is energetically more favorable to accommodate further deformation with additional in-plane strain or through local bending and surface wrinkles. Given that the particles tend to be relatively stiff and the resistance to bending of the interface relatively small, a particle-laden interface will usually buckle given enough strain [10,17]. The phenomena of buckling has been employed in previous work [10] to study the mechanical properties of the particle raft. A theoretical model of the buckling of particle-laden interfaces was presented in the same work [10]. In that model, the particles were assumed to be perfectly rigid when compared to the interface as a whole, the Poisson ratio was derived geometrically by describing the deformation of a rhombic cell, and the bending stiffness was assumed to be equivalent to that of a solid thin film of thickness equal to the diameter of the particles. Planchette et al. [22] recently showed through independent measurements of the bending stiffness of particle laden surfaces that the assumption of Vella et al. [10] capture the right scaling of the bending stiffness with particle size, but over predict its magnitude by a factor of about two. Following Vella et al.'s work [10], an estimate for the buckling wavelength is obtained:

$$\lambda = \pi\left[\frac{4}{3(1-\phi)(1+\nu)}\right]^{1/4}\sqrt{L_c d} \tag{1}$$

where ϕ is the surface coverage ratio of solids to the entire interface, ν is the estimated Poisson ratio, L_c is the capillary length of the liquid–fluid interface and d is the diameter of the particles. It was shown [10] that the prediction works well for particle diameters in the millimeter range on air–water interfaces. However, to the best of our knowledge the model for wavelength has not been tested on oil–water interfaces, or in the micron or submicron range. Here we will show that Vella et al.'s model holds for particles on an oil–water interface, but that a systematic deviation from the model occurs for particles less than one micron in diameter.

In a related field, it has been shown that the wavelength of wrinkles on a floating thin elastic sheet decays smoothly as one moves from the center of the sheet to its border, in a phenomenon called cascading [23]. Later, theory for cascading was developed based on *wrinklons*, which are defined as the localized transition region from one wavelength to another. It was also shown that the scaling for wavelength as a function of distance into the sheet depends on whether the sheet is under tension or not [24]. For a floating thin elastic sheet the tension was provided by the surface tension of the liquid acting on the edge of the sheet [23]. We will show for the first time that cascading can also occur for particle-laden interfaces and that the variation and complexity of these wrinkle transitions is amazingly rich.

Lastly, while it is known that compression affects the microscopic arrangement of particles on the interface [17], it is unclear what effects this has on the macroscopic arrangement of the particle raft on the interface or the resulting wavelength at buckling. Here we will demonstrate that the strain history of the particle raft can impact not only the uniformity of buckling across an interface, but the critical strain needed to buckle and in some instances the wavelength of the resulting wrinkles.

The objectives of this work, therefore, are manifold: to measure for the first time the buckling wavelength of particle-laden oil–water interface with particles in the sub-micron to micron range and to compare the measurements with theory; to demonstrate for the first time that cascading of wrinkles is possible on particle-laden interfaces and investigate the richness of the observed wrinkling transitions; and to understand how successive compression cycles can alter the wavelength, uniformity and critical strained needed to induce buckling.

2. Experimental setup and data collection

An acrylic Langmuir trough was used for the experiments. As presented in Fig. 1, the trough was composed of three fixed walls and a moving wall, the displacement of which was controlled by hand using a micrometer. Consequently, the strain imposed on the interface was precisely controlled, but not the strain rate. The moving wall and the fixed wall opposite to it were each fitted with a block of acrylic, which reduced the length of the interface at the middle of the raft as seen in Fig. 1. This modification increased the strain along the center of the interface compared to the edges and mitigated the effect of shear from the bounding walls. The total width of the trough was 38.1 mm and the width of the middle section was 12.7 mm. At full extension (0% compressive strain), the sides had a length of 32.0 mm and the middle section 16.0 mm.

The particles were spread on a decane–water interface. The decane was manufactured by Sigma–Aldrich (anhydrous, $\geqslant$99%)

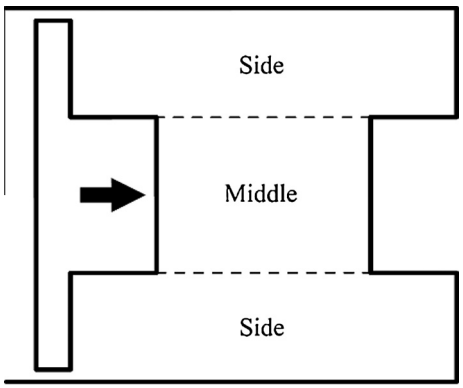

Fig. 1. Schematic representation of the Langmuir trough.

and the water was deionized at the University of Massachusetts through reverse osmosis. A 0.3 ml solution (0.1 ml of particles in water solution and 0.2 ml of water and isopropanol at 5:4 volume ratio) was used to deliver the particles to the interface. The isopropanol (Fisher Scientific®) was used as a spreading agent. Because it is miscible in both water and decane, an initially diffuse interface is generated. As the isopropanol diffuses away through the water an oil, the interface becomes sharper and a well-packed particle raft is created [16]. The effect of the isopropanol on the results are expected to be small due to its minimal final concentration in the water and oil and its high volatility. The largest particles in the present work (lycopodium powder) were sprinkled on the interface directly.

A nearly horizontal laser (Melles Griot 05-LLP-851, He–Ne) and a cylindrical lens were used to create a light sheet and illuminate the buckled interface. Imaging was done using a CMOS camera (UI-154× by iDS®, 1280 × 1024 pixels) combined with a long range microscopic lens. Each picture covered approximately 3.4 × 2.7 mm, which meant they could not cover the entire surface of the Langmuir trough. To fully image the interface, the Langmuir trough was placed on a moving stage which allowed for an array of pictures to be taken. Montages were subsequently composed using Image Magick®. The regime transition data was obtained by measuring a train of waves and dividing the resulting length by the number of wrinkles in the train. A similar approach was taken for ocean waves by Libby et al. [25]. Cascading data was obtained using a purpose-coded C++ console program. Buckled area measurements were carried out on ImageJ.

In order to study the effect of particle size on buckling wavelength and cascading, a series of spherical latex particles were used ranging in diameter from 0.1 μm to 10 μm. The size, supplier and properties of the particles used in our experiments are listed in Table 1. The contact angle of the latex particles on the decane–water interface can be found in the literature [26,27]. For the particles used in this study, a contact angle between 110° and 120° has been measured meaning they are slightly more submerged in the oil phase while trapped at the decane–water interface. These values are consistent with our measurements using the gel-trapping technique of Paunov [27]. In addition, a larger particle of lycopodium powder, D = 31 μm, were also studied. Unlike the latex particles which are essentially spherical, the lycopodium particles are more bullet-shaped with a circularity of 0.94 (standard deviation 0.02) as measured on a Nikon TE2000-U® optical microscope.

To begin the experiments, the Langmuir trough was initially filled with 24 ml of water. Next, an additional 10 ml of decane were added on top of the water. When in contact with a solid wall, the liquid interface will bend to accommodate the contact angle with the interface; this can affect the results by creating an area that is more prone to buckling than the flat interface. In order to avoid this, the walls of the Langmuir trough were designed with matching ridges and rails; these features provided a sharp angle onto which the oil–water interface could pin. At 24 ml of water, the oil–water interface was pinned to those features, but stretched into a convex shape. This resulted in a larger area available for the particles to adsorb when compared to a flat interface. With the interface in the convex configuration, 0.3 ml of particle solution were carefully injected along the interface using a syringe. The particles were observed to adsorb to the interface within a few seconds. Several minutes were allowed for the interface to form and equilibrate. To guarantee a flat interface, the excess water was then slowly removed from behind the moving wall of the Langmuir trough, which had holes drilled into it above and below the level of the interface to allow the water and oil to pass through as the interface was compressed. At this point the experiment protocol could be initiated.

Table 2 shows the strain on each part of the trough as a function of the step within the process. Initially, the interface was at 0% strain. Then, it was slowly compressed until the middle section was at 15% strain. Next, it was compressed to 32% strain. At this point, the strain was completely removed and reintroduced to 32%, so the effects of a stretching cycle on buckling could be investigated. The interface was then compressed to 49% and finally 81% strain. Then, all compressive strain was removed and partially

Table 2
Strain as a function of step.

Step	Strain	
	Side (%)	Middle (%)
1	0	0
2	8	15
3	16	32
4	0	0
5	16	32
6	24	49
7	40	81
8	0	0
9	16	32
10	24	49
11	40	81

Table 1
Properties of the particles used in the present work.

Diameter (μm)	Coefficient of variation (%)	Material	Manufacturer
0.1	NA	Sulfate latex	Invitrogen®
0.5	2.37	Polystyrene latex	Polysciences®
0.8	NA	Sulfate latex	Life Technologies®
1	0.98	Polystyrene latex	Polysciences®
1.8	5.40	White aliphatic amine latex	Invitrogen®
2.9	4.30	White sulfate polystyrene latex	Invitrogen®
10	7.69	Sulfate latex	Invitrogen®
31	7.11	Lycopodium powder	Carolina®

reintroduced to 32%, followed by 49% and 81%. The repetition of the strain history over a cycle (0–81–0–81%) allowed for the study of the effects of very high strain on the arrangement of particles and wrinkles on the interface. Images were taken at every step except those with 0% strain.

3. Results and discussion

3.1. Wavelength of buckling

Buckling wavelength measurements were performed at all steps where wrinkles were present. The wavelengths were measured in a number of different ways. Initially all wavelengths were measured manually by selecting a train of wrinkles and measuring its length and then dividing by the number of wrinkles in the train to find the wavelength. These measurements were later verified by taking a Fourier transform of each image and through a purpose-coded C++ program for select cases. The results for each of those techniques were consistent with each other and are shown in Fig. 2.

In Fig. 2, the square symbols denote the original wavelength data as measured for each of the particle rafts shown with no adjustments. From the data, it is clear that the buckling wavelengths for particles larger than one micron follow a consistent trend. However, the data points for 0.1 μm and 0.5 μm particle rafts do not follow the same trend; instead, the wavelength measured for those small particles is several times larger than expected. If the data from the particles smaller than 1 μm are excluded, the data is well fit by the theory proposed by Vella et al. [10] which showed that the wavelength should decrease steadily with diameter such that

$$\lambda \propto d^{1/2} \tag{2}$$

Three important points. First, it should be noted that these are the first measurements showing the wavelength of buckling of particle rafts on a flat oil–water interface. In Vella et al.'s [10] work, the measurements were made for particles on an air–water interface. Here we show that, for particles larger than 1 μm, Vella's [10] theory still holds for an oil–water interface. Second, the particles used by Vella et al. [10] were in the millimeter/sub-millimeter range. Here we have extended the size of the particles down to 100 nm range and have demonstrated that the theory holds for particles larger than 1 μm. Finally, we have demonstrated a transition in behavior for particle rafts composed of particles less than 1 μm. To the best of our knowledge, this transition has not been previously observed in the literature.

The literature offers a few possibilities as to the physical origin of this transition. It has been shown [21] that bidisperse solutions of 3 μm and 5 μm particles tend to organize in crystalline structures, whereas bidisperse solutions of any of those particle sizes with 9 μm particles lead to fractal structures. This was attributed to the high capillary forces acting on the 9 μm particles, and indicates that the relative magnitude of capillary and electrostatic forces may reach a tipping point in the micron range. Interestingly, fractal structures were not observed in bidisperse solutions of 1 μm and 9 μm because of the pronounced Brownian effects of the 1 μm particles. It has been shown [28] that Brownian motion is more pronounced for 0.5 μm than for 1.4 μm particles, which is evidence of the growing importance of Brownian motion in the micron range. Another possible mechanism for the transition is the formation of trilayers, which has been reported with nanoscale gold particles at an air–liquid interface [29]. The creation of a trilayer of particles leads to a higher effective bending stiffness when compared to a monolayer. Increasing the bending stiffness of the particle raft would in turn increase the wavelength of the buckling instability. It is possible that the presence of trilayers could explain the larger than expected wavelengths observed in Fig. 2 for the particles less than 1 μm. Evidence of the formation of trilayers was found on 0.1 μm-particle rafts, where, as seen in Fig. 3,

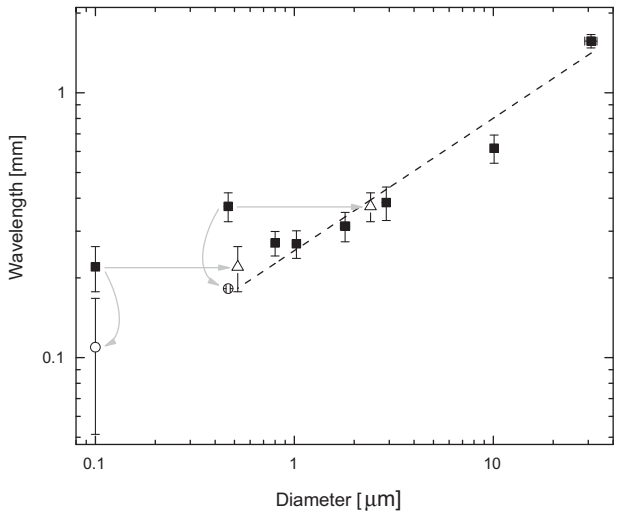

Fig. 2. Buckling wavelength of a series of particle rafts on a water–decane interface as a function of particle diameter. The squares show the original data as measured. The triangles show data for the 0.1 and 0.5 μm particles after the raft thickness has been adjusted assuming a tri-layer rather than a monolayer configuration. The circles represent the small strain results for the 0.1 μm and the 0.5 μm particles at steps 5 (32% strain) and 2 (15% strain) respectively. The dashed line is a fit to the adjusted data assuming that the wavelength scales with the square root of diameter as proposed by Vella et al. [10].

Fig. 3. Composed image showing irreversibly stacked layers of 0.1 μm particles on a particle raft after compression. The stacks are characterized by bright stripes perpendicular to the direction of compression. The stacks often occur where wrinkles formed in the previous compression cycle.

irreversible multilayers clearly form. These stacks of particles are characterized by bright regions which are often strips running perpendicular to the compression direction and often appear where wrinkles had formed during the previous compression cycles. The formation of trilayers requires that the interface initially buckles out of plane and then folds over on itself. As a result, if our trilayer hypothesis is correct, it should be possible to observe a smaller wavelength at low strains before the trilayers are formed.

In Fig. 4, the wavelength is shown as a function of step for the two particle sizes which were outside of the expected trend, 0.1 μm and 0.5 μm. Step 2 corresponds to the lowest global strain imposed on the sheet at only 15%. For the 0.5 μm particles the wavelength of wrinkling measured at step 2 is significantly smaller than all the other larger strain cases. In fact it is reduced by more than a factor of two. This suggests that, as hypothesized, the trilayers may not have formed yet at this small strain. In fact, if the wavelength measured for the 0.5 μm particles at small strain is superimposed on the data in Fig. 2, the data collapses with the large particle data and fits very well onto the line representing Vella et al.'s [10] theory. Thus, there is strong evidence that trilayers do form on the 0.5 μm particle case. The evidence for the 0.1 μm case is not as clear. At step 2, the measured wavelength is reduced, but not by enough to fit the line. This may be because although the global strain is small, the particle distribution is not uniform and the strain can become localized. As a result, very little of the interface is observed to buckle. As we will address later, successive compressions can rearrange and realign particles on the interface to make the raft more homogenously packed and the imposed strains more uniform. Thus although the strain at step 5 is larger than step 2, the fraction of the surface buckling is significantly larger and the local strain may be in fact much less. The wavelength measured at step 5 for 0.1 μm particle rafts is also significantly smaller than at larger strains and again fits the Vella et al. [10] predictions for a monolayer of particles very well. This also applies to step 7 on the 0.5 μm data; the wavelength is approximately the same as in step 2, but the strain is much larger. However, it was found that most of the strain was focused into folds, and that the wrinkles that could be measured at that global strain were actually at a much lower local strain. This situation is exemplified in Fig. 5. In the figure, area A is characterized by folding of the interface with high local strain compared to the global strain. The nearby areas marked with a B are wrinkled, but no folding occurs, which indicates that the local strain is smaller here than in area A. Finally,

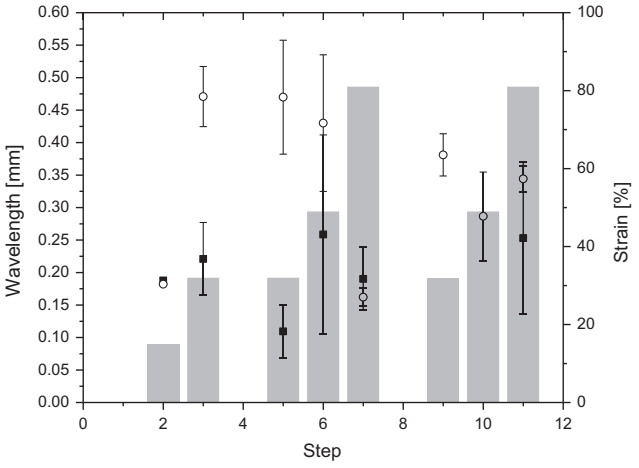

Fig. 4. Buckling wavelength and compressive strain as a function of the step in the experimental protocol shown in Table 2 for the 0.1 μm (squares) and 0.5 μm (circles) diameter particles. In the figure, the symbols indicate the wavelength while the columns represent the percent strain at a given step.

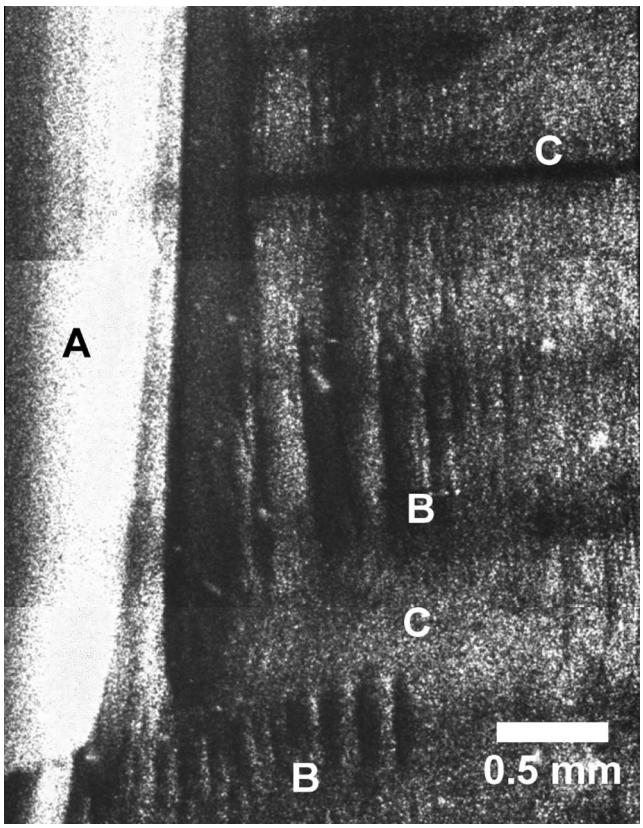

Fig. 5. Section of a 0.5 μm particle raft at step 7 (81% strain). Despite the large global strain, not all areas are under high local strain. (A) Folds, very high local strain; (B) Small wrinkles whose wavelength was measured, lower local strain; (C) Flat area, very low local strain. The dark horizontal lines are shaded areas with low incidence of the laser sheet. Three images were stacked vertically to compose this image; the transitions between them can be seen just above A and on the lower C area.

the areas marked with a C are flat and are therefore under even lower local strain.

Now, we propose a simple modification to the theory of Vella et al. [10] to accommodate for the formation of trilayers. In that work, the thickness of the sheet was assumed to be equal to the diameter of the particle raft. Without that assumption, the wavelength may be estimated by:

$$\lambda = \pi\left[\frac{4}{3(1-\phi)(1-\nu)}\right]^{1/4}\left(\frac{t^3}{d}\right)^{1/4} L_c^{1/2} \tag{3}$$

where ϕ is the solid area ratio of the interface, ν is the Poisson ratio, t is the thickness of the interface, d is the diameter of the particles and L_c is the capillary length. Then, a trilayer can be said to behave approximately as a single layer with an "effective" diameter of:

$$d_{\text{eff}} = m^{3/2} d \tag{4}$$

where m is the number of layers in the stack. The number of layers is expected to be an odd number if our physical model of buckling and then folding over is to hold. For a trilayers, this yields an effective diameter of:

$$d_{\text{eff}} \cong 5.2d \tag{5}$$

Using this formula for the effective diameter of a trilayer, the data for the 0.1 μm and 0.5 μm particles can be shifted to 0.52 μm and 2.4 μm respectively. These data points (denoted by triangles) have been superimposed over the data in Fig. 2. Using the effective diameter for the two cases below 1 μm, all of the data collapses

onto the same power law curve. This gives additional support to the hypothesis that the transition observed between regimes for particles less than a micron is the result of a shift in the mechanism of buckling, from the buckling of a monolayer of particles to the formation of trilayers.

3.2. Cascading in particle-laden Interfaces

Areas of different wavelength often occur on the same particle raft. In those cases, the interface must deform in such a way as to accommodate both wavelengths. This transition was observed to occur in a number of different ways, all of which are represented in Fig. 6. They include:

Fig. 6a: One wrinkle splits into two wrinkles. This usually occurs in the middle of a buckled area. Transitions from one to two wrinkles have been proposed to be the building block of the global transition between wavelengths [24]. Thus, this kind of transition does not differ fundamentally from what is observed in thin solid sheets.
Fig. 6b: A wrinkle simply ends at the edge of a buckled area, without any transition to a smaller wavelength. This often happens in areas where other wrinkles split into smaller wavelengths, which suggests that some stress is released. Since the wavelength at the edge of the buckled area (or, equivalently, at the edge of a thin solid sheet) is a function of the stress state in that region, the fact that wrinkles can end abruptly does not mean that the particle-laden interface behaves in any way differently from thin solid sheets.
Fig. 6c: One wrinkle splits into between three and six short wrinkles. This usually occurs at the edges of buckled areas. This has not been reported for thin solid sheets, so it is likely limited to particle-laden interfaces.
Fig. 6d: A flat area develops between the two wavelengths that are to be connected. This phenomenon has been found to occur when two areas that were previously buckled are pushed together due to additional compression of the particle raft, nearly (but not completely) eliminating the flat area between them. This also appears to be particular to particle-laden interfaces.
Fig. 6e: A sharp fault-like transition develops. This is characterized by a discontinuity in wavelength and possible rupture of the particle raft. This likely occurs where discontinuities in packing or grain boundaries in the particle raft occur and has not been reported for thin solid sheets.
Fig. 6f: The wavelength transitions smoothly from one value to the other. This occurs via numerous discrete transitions over a large area of the interface. Although each transition is discrete, the average wavelength varies smoothly due to the large number of transitions.
Case *f* is characterized by an apparently continuous transition between wavelengths similar to the cascading observed in thin solid sheets. We now move on to characterizing the instances of case *f* in the present work.

The smoothness of the transition between wavelengths can be measured by calculating the average wavelength, λ_{avg}, over a line parallel to the edge of the sheet as a function of the distance, *y*,

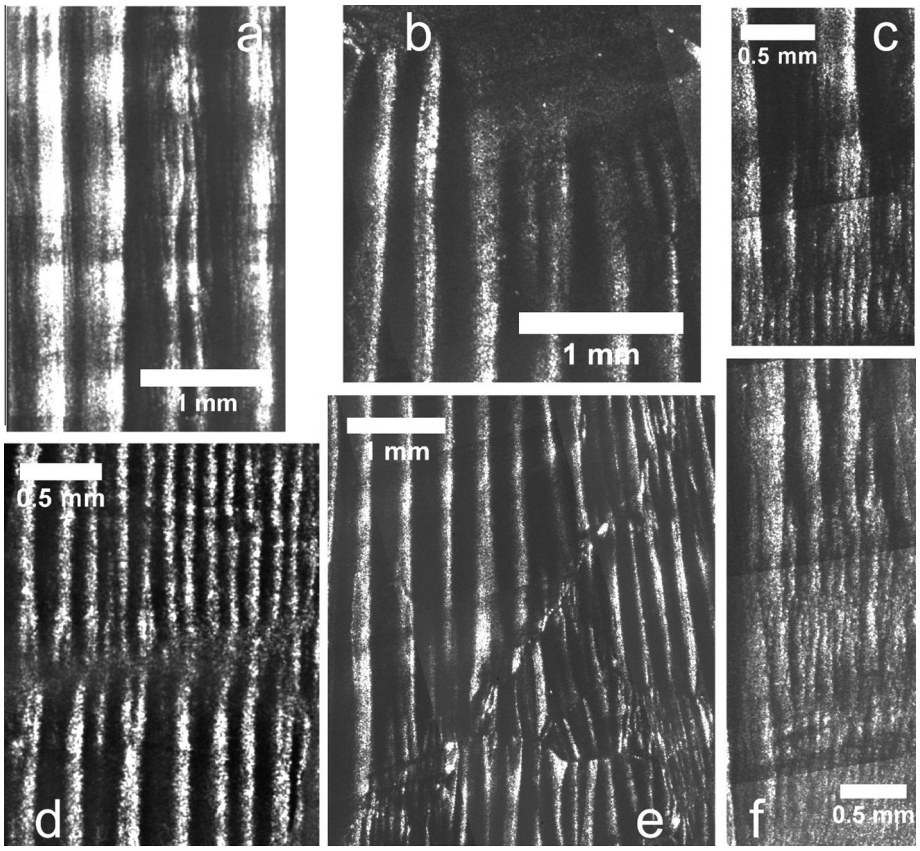

Fig. 6. Wavelength transition events in particle-laden interfaces: (a) A wrinkle splits into two wrinkles, 1.8 μm particle raft; (b) Wrinkles end abruptly at the end of a buckled area, while other wrinkles split before ending, 0.8 μm particle raft; (c) A wrinkle splits into five wrinkles at the edge of a buckled area, 0.5 μm particle raft; (d) The transition between the wrinkles at the top and bottom occurs through a flat area on this 1.0 μm particle raft; (e) Fault-like transition on a 0.8 μm particle raft; (f) Gradual transition from a large wavelength to a much smaller wavelength, then a sudden transition to no buckling. 2.9 μm particle raft.

from that line to the edge of the sheet [24]. An equivalent approach would be to work with the average wave number [23]. The scaling for wavelength with distance from the edge of the sheet should be [24]:

$$\lambda_{\text{light}} \propto y^{2/3} \tag{6}$$

$$\lambda_{\text{heavy}} \propto y^{1/2} \tag{7}$$

where "light" refers to sheets under negligible lateral tension and "heavy" refers to sheets under considerable tension. This terminology comes from observations of wavelength variation along hanging drapes and curtains [24]. The tension smoothens out the transition because it makes it energetically unfavorable to focus the curvature on a single point. Therefore, "heavy" sheets are characterized by smoother transitions than "light" sheets, as it is reflected on the scaling in Eqs. (6) and (7).

It should be pointed out that cascading is, at the most basic level, the collection of several different divisions of wrinkles into two wrinkles of smaller wavelength. Consequently, the continuous trends expected in the theory could only be obtained if a sheet or raft of infinite width were to be measured. For real data measured from a finite particle raft, discontinuities in the average wavelength are to be expected. This is an important issue because the regions of cascading tend to be small in particle-laden interfaces. Another important issue is that the end of the raft cannot be easily identified. Consequently, the distance from the edge of the raft, y, was measured from the nearest flat region in the particle raft.

The wavelength was measured using automated image processing, and the wavelength at each position, y, was averaged to obtain the wavelength at each location. This was done for every occurrence of cascading that was identified in the present work. An example of the data that was obtained is shown in Fig. 7.

Each cascading event was then analyzed individually. This was done by obtaining the scaling for each event after subtracting the minimum wavelength for that particular event. In other words, all wavelength-to-y curves were set to start at approximately zero; this removed the influence of the sudden increase in wavelength from the flat area to the buckled area. Mathematically, the wavelength was assumed to be of the form:

$$\lambda = \lambda_{\min} + ay^m \tag{8}$$

Applying this process to each cascading event detected in the data led to a probability distribution for the exponent m. The mean for this distribution is approximately 0.47, however, the distribution was quite broad with a standard deviation of 0.22 (i.e., the coefficient of variation is approximately 46%). The mode is at 0.40 and the median at 0.44. This indicates a slightly skewed distribution, but these values compare favorably with the value of 0.5 for "heavy" sheets proposed by Leahy et al. [29]. This observation suggests the particle rafts are under tension. Huang showed that the influence of surface tension on the edge of a thin polymer sheet was adequate to obtain an exponent of $m = 0.5$. It is likely that surface tension is also putting the particle rafts in tension in regions of low particle concentration where the wrinkles terminate. Furthermore, a relatively wide tail in the distribution at large values of m indicates the occurrence of occasional "light" sheet behavior as well.

Thus, it can be said that the cascading of particle-laden interfaces is similar to that of thin solid sheets, in that the wavelength transition can be smooth ("heavy sheet behavior" – under lateral tension) or sharp ("light sheet behavior" – no lateral tension). Furthermore, it is clear that most often this transition is smooth. Other exponents that indicate neither kind of behavior are also obtained, most likely caused by numerical error due to the use of relatively small data sets.

Still, the wavelength transitions in particle-laden interfaces are not limited to the behaviors observed for thin solid sheets. As presented in Fig. 6c–e, there are a number of classes of cascading events observed for the first time on particle rafts. Thus, a fundamental difference in behavior from solid sheets has been demonstrated. This points to a series of new physical mechanisms that allow such varied behavior, including: particle rafts can rearrange and realign under stress, which means dislocations can be added and removed simply by compressing the raft; the size of the particles is an inherent limitation to the curvature of the sheet; the raft is not continuous upon injection of the particles; and the shear from the side walls plays a role, while in floating thin sheets it can be entirely avoided.

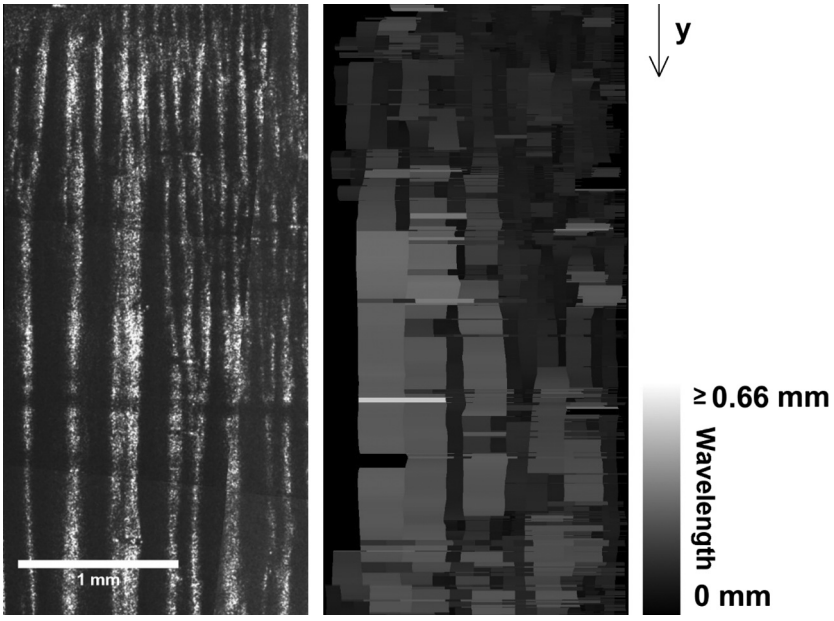

Fig. 7. Example of cascading (left) and corresponding image processing output showing the local wavelength as a grayscale color map. The raft is composed of 1.0 μm particles.

3.3. Hysteresis in particle-laden Interfaces

Particles are bound to the interface by the interplay between electrostatic and capillary effects. Consequently, the energy input that is necessary to promote changes in structure is small when compared to regular solids, where the molecules are bound by intermolecular forces. This is particularly true for interfaces below optimum packing. Therefore, some change in behavior between successive compression cycles ought to be expected.

Fig. 8 shows an example of the effects of hysteresis on a 1.0 μm-particle-laden interface over steps 3, 5 and 9 of the experimental protocol, all of which are at 32% strain. The buckled area of the interface increases slightly between steps 3 and 5, where the strain goes from 32% to 0% then back to 32%, and there is no buckling at all at step 9, where the strain was increased from 32% to 81%, then down to 0% and back to 32%. Additionally, the wrinkles are originally tilted in relation to the direction of compression, but this misalignment is mostly eliminated between steps 3 and 5. Lastly, the spatial distribution of the wrinkles changes between steps 3 and 5, i.e., wrinkles form where they did not before or cease to exist in a certain part of the sheet. This indicates that the arrangement of the particles on the interface is modified by compression, which leads to hysteretic behavior.

One way to quantify the hysteresis of particle laden interfaces is by determining the percentage of the interface that has wrinkled at each step of the experimental protocol. This was measured in ImageJ. Note that only the surface area captured by the camera was analyzed. These measurements yield the data in Fig. 9. Interestingly, the change in percentage of surface wrinkling is small between steps 3 and 5, which are characterized by the same strain (32%), but between which the compression is completely released to 0% and reintroduced to 32%. That indicates that little change in the arrangement of the particles has occurred between these steps. This is not to say that there is no effect at all; in fact, areas of poor particle coverage often move between steps 3 and 5, and the spatial distribution and alignment of the wrinkles tends to change as well. However, the amount of the interface that has buckled does not change, which shows that the effective length of the interface did not change.

On the other hand, the percentage of the particle raft that wrinkles tends to be small in step 9 when compared to steps 3 and 5, even though it is at the same strain. The interface is at 32% strain in step 5, then it is put under very high strain (81%), which is then released to 0% and partially reapplied back to 32% at step 9. The difference in behavior between these two steps thus indicates that high compression can induce changes in particle arrangement. These changes between steps 5 and 9 may be due to a number of reasons including: forcing closer packing of the particles; populating previously unpopulated areas of the trough; or irreversible formation of trilayers of particles that effectively reduce the length of the interface. We do not believe particles are driven off the interface to any relevant degree, since they are strongly bound to the interface by capillary forces.

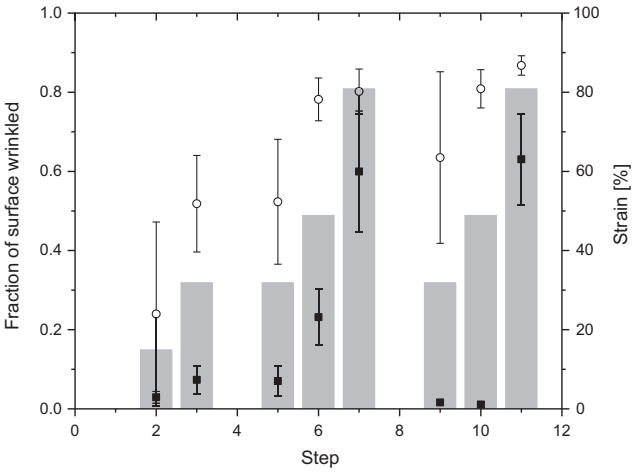

Fig. 9. The fraction of the particle-laden interface that wrinkled and compressive strain as a function of step in the experimental protocol shown in Table 2 for the 0.1 μm (squares) and 0.5 μm (circles) diameter particles. The 0.5 μm data was found to be representative of the larger diameters, which are not shown here for the sake of simplicity. In the figure, the symbols indicate the wavelength while the columns represent the percent strain at a given step.

It is unlikely that changes in packing at microscopic level played a role, since buckling requires that the particles be very closely packed in the first place. The irreversible formation of trilayers is also an unlikely reason for the observed behavior, since that was only observed for the 0.1 μm particles, and even then only on a small portion of the interface. Thus, hysteresis is likely due to populating previously unpopulated areas of the trough, i.e., macroscopic rearrangement of the particles. Indeed, evidence of that is found both in the uneven buckling of interfaces observed in Fig. 5 and in the empty areas that often form after the particles are injected.

It should be pointed out that these spreading issues are rare with the 31 μm particles, because they were not injected but instead sprinkled on top of the interface. This makes the initial spreading more even and thus less likely to lead to uneven buckling. This supports spreading as a favorable way of depositing particles on the interface. When uneven spreading does occur, the particle-laden interfaces tend to become more homogeneous when large strains are imposed. Therefore, the reproducibility of the interfaces increases with the use of hysteresis, which is important both in scientific experiments and in industrial processes.

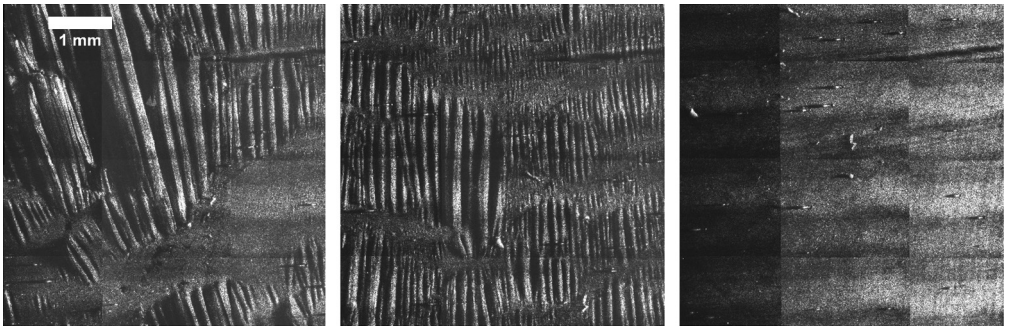

Fig. 8. Hysteresis on a 1.0 μm-particle raft; numbers represent the step in the protocol. All images show the same area of the raft at 32% strain. From left to right: step 3, 5 and 9. Between steps 3 and 5, the interface is decompressed to 0% and compressed back to 32%. Between steps 5 and 9, the interface is compressed to 81%, then decompressed to 0%, and recompressed to 32%.

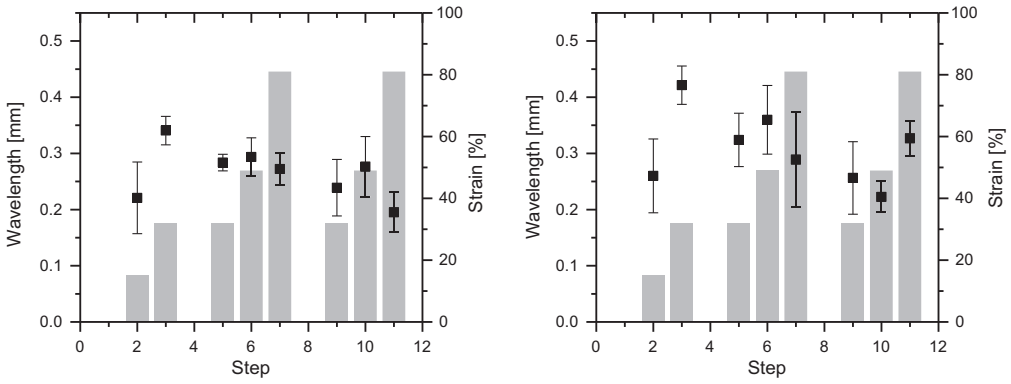

Fig. 10. Wavelength and strain as a function of step for the 0.8 μm (left) and the 1.8 μm (right) particles. Within measurement error, the wavelength is constant as a function of step. This data is representative of the larger particles in this work. In the figure, the symbols indicate the wavelength while the columns represent the percent strain at a given step.

Yet, it is important to consider whether imposing strain in order to induce hysteresis can also affect the mechanical properties of the interface. Since the wavelength of buckling is expected to be linked to the bending stiffness of the material, it can give an indication of the variation of the latter. In Fig. 10, the wavelength is shown as a function of step for the 0.8 μm and the 1.8 μm particles. While some variation is observed, the wavelength seems to gravitate around an average for all cases shown here. This indicates that the change in mechanical properties, if any, is very small. The data sets in Fig. 10 are representative of the remaining particle diameters, with the exception of the 0.1 μm and the 0.5 μm particles.

4. Conclusions

In the present work, the buckling of an oil–water interface was investigated using a Langmuir trough. Polystyrene particles with diameters ranging from 0.1 μm to 10 μm were used, as well as lycopodium particles of 31 μm in diameter. The interface was put through 3 compression cycles of varying strains, and images of the interface were recorded at predefined steps. The wavelength of buckling and the areal distribution of wrinkles on the interface were measured, and results were presented based on those measurements. These measurements extended the previous work in the literature [10] to smaller diameter particles and to an oil–water interface.

Our measurements of the wavelength of buckling of particle-laden interfaces demonstrate that the scaling of wavelength with particle diameter predicted by Vella et al. [10] can be applied to micron-sized particles on an oil–water interface. However, for particles with a diameter less than 0.8 μm, a deviation from the experimental trends and the theoretical predictions were observed. For these sub-micron particles, the buckling wavelengths were much larger than those predicted by the theory of Vella et al. [10] suggesting an interface with a larger than expected bending stiffness. We postulated that the observed deviation in the data occurs because the particle laden interface first deforms and stacks into trilayers before subsequently buckling. Due to its increased thickness, a tri-layer will have a significantly larger bending stiffness than a monolayer. As a result, if one uses the thickness of the tri-layer rather than the particle diameter in the scaling of Vella et al. [10], the data for the sub-micron particles collapse onto the experimental trends observed for the larger particles and the theoretical predictions of buckling wavelength. Additionally, similar tri-layers of gold nanoparticles have been observed by Leahy et al. [29]. A number of interesting open questions still exist including how the particle density and charge, interfacial tension, salinity, etc. affect the critical diameter of the observed transition.

In this study, we showed that different wavelengths can occur across a particle-laden interface. These wavelength variations can be the result of the inhomogeneous initial particle loading which is made more uniform with multiple compression cycles. However, transition between different wavelengths were also for the first time observed due to wavelength cascading like that which has been observed in thin solid sheets floating on a liquid interface [23,30]. Both "light" and "heavy" sheet behavior are possible depending on the amount of tension applied normal to the compression direction applied either via surface tension or gravity [23,24]. For the particle laden interfaces studied here, a "heavy" or high tension response was most often observed, but a broad distribution of cascading phenomena was apparent with a much richer array of wrinkling transitions than has been observed for thin films.

The transition between different wavelengths within a buckled raft was found to occur in a number of completely novel ways. In one of those cases, a flat area remains between two trains of wrinkles, allowing for the misalignment of the crests. Another possibility is that a very pronounced discontinuity may form along the raft, with different wavelengths on either side. Lastly, a single wrinkle was observed to split into up to six smaller wrinkles. None of these cases has been reported in thin solid sheets and they are likely the result of the discrete nature of the particles and possibly the presence of grain boundaries between isolated particle rafts that are pressed together during compression.

Finally, from this work, we were able to demonstrate that compression can be used to efficiently change the particle distribution on the interface, especially if large compressive strains are imposed on the particle raft. This could be particularly useful in applications where the particles must be injected (as opposed to sprinkled) on the interface. The small changes in wavelength between compression cycles suggest that the bending stiffness of the interface remains unchanged by the process, even as the percent of the surface that buckled varied between compression cycles.

Acknowledgments

The authors would like to thank the National Science Foundation for support of this research through the Materials Research Science and Engineering Center on Polymers (DMR-0820506) at the University of Massachusetts.

References

[1] B.P. Binks, Curr. Opin. Colloid Interface Sci. 7 (2002) 21–41.
[2] S.U. Pickering, J. Chem. Soc., Trans. 91 (1907) 2001–2021.
[3] N.P. Ashby, B.P. Binks, Phys. Chem. Chem. Phys. 2 (2000) 5640–5646.

[4] K.V. Edmond, M. Marquez, A.B. Schofield, J.P. Rothstein, A.D. Dinsmore, Langmuir 22 (2006) 9052–9056.
[5] M. Mulligan, J.P. Rothstein, Langmuir 27 (2011) 9760–9768.
[6] A.D. Dinsmore, M.F. Hsu, M.G. Nikolaides, M. Marquez, A.R. Bausch, D.A. Weitz, Science 298 (2002) 1006–1009.
[7] K.S. Birdi, Handbook of Surface and Colloid Chemistry, second ed., CRC Press, New York, 1994.
[8] M.P. Boneva, N.C. Christov, K.D. Danov, P.A. Kralchevsky, Phys. Chem. Chem. Phys. 9 (2007) 6371–6384.
[9] M. Oettel, S. Dietrich, Langmuir 24 (2008) 1425–1441.
[10] D. Vella, P. Aussillous, L. Mahadevan, Europhys. Lett. 68 (2004) 212–218.
[11] C. Zeng, H. Bissig, A.D. Dinsmore, Solid State Commun. 139 (2006) 547–556.
[12] R. Daniello, M. Donnell, K. Khan, J.P. Rothstein, Phys. Rev. E 89 (2014) 023014.
[13] D. Vella, L. Mahadevan, Am. J. Phys. 73 (2005) 817–825.
[14] P.A. Kralchevsky, K. Nagayama, Adv. Colloid Int. Sci. 85 (2000) 145–192.
[15] M.G. Nikolaides, A.R. Bausch, M.F. Hsu, A.D. Dinsmore, M.P. Brenner, C. Gay, D.A. Weitz, Nature 420 (2002) 299–301.
[16] S. Reynaert, P. Moldenaers, J. Vermant, Langmuir 22 (2006) 4936–4945.
[17] R. Aveyard, J.H. Clint, D. Nees, V.N. Paunov, Langmuir 16 (2000) 1969–1979.
[18] A. Moncho-Jorda, F. Martınez-Lopez, A.E. Gonzalez, R. Hidalgo-Alvarez, Langmuir 18 (2002) 9183–9191.
[19] P. Pieranski, Phys. Rev. Lett. 45 (1980) 569–572.
[20] C. Monteux, J. Kirkwood, H. Xu, E. Jung, G.G. Fuller, Phys. Chem. Chem. Phys. 9 (2007) 6344–6350.
[21] C. Monteux, E. Jung, G.G. Fuller, Langmuir 23 (2007) 3975–3980.
[22] C. Planchette, E. Lorenceau, A.-L. Biance, Soft Matter 8 (2012) 2444–2451.
[23] J. Huang, B. Davidovitch, C.D. Santangelo, T.P. Russell, N. Menon1, Phys. Rev. Lett. 105 (2010) 038302.
[24] H. Vandeparre, M. Piñeirua, F. Brau, B. Roman, J. Bico, C. Gay, W. Bao, C.N. Lau, P.M. Reis, P. Damman, Phys. Rev. Lett. 106 (2011) 224301.
[25] L.M. Libby, W.F. Libby, S.S. Lawrence, Measurement of Ocean Waves in a Satellite Photograph, Rand Corp, New York, 1969.
[26] B.J. Park, J.P. Pantina, E.M. Furst, M. Oettel, S. Reynaert, J. Vermant, Langmuir 24 (2008) 1686–1694.
[27] V.N. Paunov, Langmuir 19 (2003) 7970–7976.
[28] L.E. Helseth, R. Muruganathan, Y. Zhang, T.M. Fischer, Langmuir 21 (2005) 7271–7275.
[29] B.D. Leahy, L. Pocivavsek, M. Meron, K.L. Lam, D. Salas, P.J. Viccaro, K.Y.C. Lee, B. Lin, Phys. Rev. Lett. 105 (2010) 058301.
[30] J. Huang, M. Juszkiewicz, W.H.d. Jeu, E. Cerda, T. Emrick, N. Menon, T.P. Russell, Science 317 (2007) 650–653.